ROYAL SOCIETY OPEN SCIENCE

rsos.royalsocietypublishing.org

Research

Cite this article: Aoyagi S, Miwa K, Ueno H, Okada H, Matsuo Y, Kokubo K. 2018 Structure of [60]fullerene with a mobile lithium cation inside. *R. Soc. open sci.* **5**: 180337. http://dx.doi.org/10.1098/rsos.180337

Received: 1 March 2018
Accepted: 4 June 2018

Subject Category:
Chemistry

Subject Areas:
materials science

Keywords:
fullerene, endohedral metallofullerene, $Li^+@C_{60}$, X-ray crystal structure analysis, synchrotron radiation

Author for correspondence:
e-mail: aoyagi@nsc.nagoya-cu.ac.jp

†Present address: CNT-Application Research Center, National Institute of Advanced Industrial Science and Technology (AIST), Tsukuba, Ibaraki 305-8565, Japan.

This article has been edited by the Royal Society of Chemistry, including the commissioning, peer review process and editorial aspects up to the point of acceptance.

Electronic supplementary material is available online at https://dx.doi.org/10.6084/m9.figshare.c.4153670.

THE ROYAL SOCIETY PUBLISHING

Structure of [60]fullerene with a mobile lithium cation inside

Shinobu Aoyagi[1], Kazuhira Miwa[1], Hiroshi Ueno[2], Hiroshi Okada[3], Yutaka Matsuo[2,3,4] and Ken Kokubo[5,†]

[1]Department of Information and Basic Science, Nagoya City University, Nagoya 467-8501, Japan
[2]School of Chemistry, Northeast Normal University, 5268 Renmin Street, Changchun, Jilin 130024, People's Republic of China
[3]Department of Mechanical Engineering, School of Engineering, The University of Tokyo, 7-3-1 Hongo, Bunkyo-ku, Tokyo 113-8656, Japan
[4]Hefei National Laboratory for Physical Sciences at the Microscale, University of Science and Technology of China, 96 Jinzhai Road, Hefei, Anhui 230026, People's Republic of China
[5]Division of Applied Chemistry, Graduate School of Engineering, Osaka University, Suita, Osaka 565-0871, Japan

SA, 0000-0002-7393-343X; HO, 0000-0002-0809-8167; YM, 0000-0001-9084-9670; KK, 0000-0002-8776-7102

The structure of crystalline [60]fullerene with a lithium cation inside ($Li^+@C_{60}$) was determined by synchrotron radiation X-ray diffraction measurements to understand the electrostatic and thermal properties of the encapsulated Li^+ cation. Although the C_{60} cages show severe orientation disorder in $[Li^+@C_{60}](TFPB^-)\cdot C_4H_{10}O$ and $[Li^+@C_{60}](TFSI^-)\cdot CH_2Cl_2$, the Li^+ cations are rather ordered at specific positions by electrostatic interactions with coordinated anions outside the C_{60} cage. The $Li^+@C_{60}$ molecules in $[Li^+@C_{60}](ClO_4^-)$ with a rock-salt-type cubic structure are fully disordered with almost uniform spherical shell charge densities even at 100 K by octahedral coordination of ClO_4^- tetrahedra and show no orientation ordering, unlike $[Li^+@C_{60}](PF_6^-)$ and pristine C_{60}. Single-bonded $(Li^+@C_{60}^-)_2$ dimers in $[Li^+@C_{60}^-](NiOEP)\cdot CH_2Cl_2$ are thermally stable even at 400 K and form Li^+–C bonds which are shorter than Li^+–C bonds in $[Li^+@C_{60}](PF_6^-)$ and suppress the rotational motion of the Li^+ cations.

1. Introduction

Hollow spherical carbon molecules called fullerenes or buckyballs with a molecular formula of C_{2n} ($n \geq 30$) can contain various atoms and molecules [1,2]. Endohedral fullerenes containing

atoms and molecules with magnetic and electric moments have the potential to be used for molecular devices such as quantum bits [3,4], magnetic resonance imaging agents [5,6] and molecular switches [7,8]. [60]Fullerene C_{60} with a soccer-ball shape of 1 nm diameter is the most abundant fullerene in soot obtained by arc discharge of graphite electrodes and is valuable in applications such as solar cells [9,10]. Endohedral C_{60} with a lithium cation inside ($Li^+@C_{60}$) is efficiently obtained by lithium plasma bombardment with C_{60} vapour onto a target plate and is commercially available from Idea International Co., Ltd. [11–13]. It has been reported that $Li^+@C_{60}$ shows outstanding electron-accepting properties for applications such as photoelectrochemical solar cells [14–16] and non-volatile organic transistor-based memories [17].

$Li^+@C_{60}$ forms crystalline salts with anions such as $SbCl_6^-$ and PF_6^- [11,18]. The PF_6^- salt, $[Li^+@C_{60}](PF_6^-)$, has a rock-salt-type cubic structure and shows a fast response to an alternating electric field by free rotational motion of the Li^+ cation on a shell with a radius of 1.5 Å inside the C_{60} cage [18–20]. The free rotational motion of the Li^+ cation is suppressed so that it is localized at two off-centre equivalent positions on the threefold inversion axis of the cubic crystal below 100 K. The simultaneous occupation of the two positions at low temperature is attributed to a quantum tunnelling of the Li^+ cation between the two positions with an interval of 2.7 Å. The tunnelling motion is also hindered below $T_C = 24$ K with an abrupt decrease in the dielectric permittivity by antiferroelectric interactions among local electric dipole moments formed between the Li^+ cations inside and the PF_6^- anions outside the C_{60} cages. The tunnelling motion and intermolecular interaction of the Li^+ cation suggest that $Li^+@C_{60}$ has the potential to be used as a quantum bit in quantum computers using electric dipole moments.

The position and motion of a Li^+ cation inside C_{60} are significantly affected by the coordinated anions and molecules outside the C_{60}. For instance, the Li^+ cation in the $SbCl_6^-$ salt is localized at two adjoining off-centre positions at 370 K by asymmetric coordination of $SbCl_6^-$ anions around an $Li^+@C_{60}$ molecule [11]. Such anion exchange effects should be investigated in more depth to understand the electrostatic responses of the encapsulated Li^+ cations. Crystals of $[Li^+@C_{60}](PF_6^-)$, $[Li^+@C_{60}](SbCl_6^-)$ and $[Li^+@C_{60}](TFPB^-)$ (TFPB, tetrakis{3,5-bis(trifluoromethyl)phenyl}borate) were previously obtained and structurally characterized [11,18,21]. Further structural study of $[Li^+@C_{60}](TFPB^-)$ is required, because the position and motion of the Li^+ cation have not been revealed in the previous structural analysis [21]. The anions of the previously obtained crystals are all non-polar. $Li^+@C_{60}$ crystals combined with polar anions such as $TFSI^-$ (TFSI, bis(trifluoromethylsulfonyl)imide) should also be obtained and structurally characterized. PF_6^- and $SbCl_6^-$ are small octahedral anions, whereas $TFPB^-$ is a large tetrahedral anion. It is worthwhile obtaining and investigating $Li^+@C_{60}$ crystals combined with small tetrahedral anions such as ClO_4^-. A crystal of dimerized $Li^+@C_{60}^-$ without anions was also obtained by electrochemical reduction [22]. The crystal is different from other dimerized endohedral metallofullerene crystals that consist of negatively charged endohedral metallofullerenes and positively charged donor molecules [23,24]. The Li^+ cation in the dimerized $Li^+@C_{60}^-$ is localized near the carbon atom that is nearest to the carbon atom forming an inter-fullerene single C–C bond at 100 K. Temperature dependence of the position and motion of the localized Li^+ cation in the dimerized $Li^+@C_{60}^-$ would provide us with essential information about the thermal stability of the $(Li^+@C_{60}^-)_2$ dimer and the Li^+–C bond.

To understand the electrostatic and thermal properties of the mobile Li^+ cation inside C_{60}, we investigated the effects of the coordination structure and temperature on the position and motion of the encapsulated Li^+ cations in $Li^+@C_{60}$ crystals by synchrotron radiation (SR) X-ray structure analysis in this study.

2. Material and methods

We performed the X-ray crystal structure analyses of $[Li^+@C_{60}](TFPB^-)$, $[Li^+@C_{60}](TFSI^-)$, $[Li^+@C_{60}](ClO_4^-)$ and $[Li^+@C_{60}^-](NiOEP)$ (OEP, octaethylpolphyrine). The $TFPB^-$, $TFSI^-$ and ClO_4^- salts were obtained by anion exchange of $[Li^+@C_{60}](PF_6^-)$ [21]. Single crystals of the $TFPB^-$ and $TFSI^-$ salts and powder crystals of the ClO_4^- salt were obtained by vapour diffusion from solutions. The crystal structure of $[Li^+@C_{60}](TFPB^-)$ without solvent molecules at 123 K has already been reported [21]. A single crystal of $[Li^+@C_{60}](TFPB^-)$ containing diethyl ether solvent molecules was obtained in this study. Single crystals of $[Li^+@C_{60}^-](NiOEP)$ were obtained by electrochemical reduction in $[Li^+@C_{60}](TFSI^-)$ solution in the presence of NiOEP [22]. The crystal structure of $[Li^+@C_{60}^-](NiOEP)$ containing dichloromethane solvent molecules at 100 and 250 K has already been reported [22]. We report the crystal structure of $[Li^+@C_{60}^-](NiOEP)$ at 400 K and discuss the temperature dependence of the crystal structure in this study. The SR X-ray diffraction (XRD) measurements were performed

Table 1. Experimental conditions and crystallographic data. The reliable factors based on absolute structure factors (R) and the weighted reliable factors based on squared structure factors (R_w) are given for the single-crystal structure refinements of [Li^+@C_{60}]($TFPB^-$), [Li^+@C_{60}]($TFSI^-$) and [Li^+@$C_{60}{}^-$](NiOEP). The weighted profile reliable factor (R_{wp}) and the reliable factor based on Bragg intensities (R_I) are given for the Rietveld refinement of [Li^+@C_{60}]($ClO_4{}^-$).

	[Li^+@C_{60}]($TFPB^-$)	[Li^+@C_{60}]($TFSI^-$)	[Li^+@C_{60}]($ClO_4{}^-$)	[Li^+@$C_{60}{}^-$](NiOEP)
formula	$LiC_{60}\cdot C_{32}H_{12}BF_{24}\cdot C_4H_{10}O$	$LiC_{60}\cdot C_2F_6NO_4S_2\cdot CH_2Cl_2$	$LiC_{60}\cdot O_4Cl$	$LiC_{60}\cdot NiC_{36}N_4H_{44}\cdot CH_2Cl_2$
formula weight	1664.88	1092.62	827.03	1403.93
crystal size (mm)	0.25 × 0.12 × 0.11	0.30 × 0.08 × 0.04	powder	0.25 × 0.03 × 0.03
temperature (K)	260	150	30–450	400
X-ray wavelength (Å)	0.41324	0.70220	0.64898	0.41400
crystal system	monoclinic	orthorhombic	cubic	monoclinic
space group	$P2_1/c$	$Pnma$	$Fm\bar{3}m$	$C2/m$
unit cell parameters	$a = 17.1122(9)$ Å	$a = 18.963(5)$ Å	$a = 14.133(1)$ Å	$a = 24.6791(13)$ Å
	$b = 20.3829(12)$ Å	$b = 13.892(3)$ Å	$V = 2822.9(6)$ Å^3	$b = 14.9697(6)$ Å
	$c = 19.8912(18)$ Å	$c = 13.964(3)$ Å	(100 K)	$c = 17.7061(15)$ Å
	$\beta = 105.157(5)°$	$V = 3678.5(15)$ Å^3		$\beta = 109.171(5)°$
	$V = 6696.6(8)$ Å^3			$V = 6178.5(7)$ Å^3
Z	4	4	4	4
no. of independent reflections	13 115 ($d > 0.80$ Å)	3684 ($d > 0.78$ Å)	162 ($d > 0.85$ Å) (1434 data points)	8779 ($d > 0.70$ Å)
no. of parameters	1459	433	55	657
reliable factors	$R = 0.125$ ($\|F\| > 4\sigma$)	$R = 0.098$ ($\|F\| > 4\sigma$)	$R_{wp} = 0.036$ (100 K)	$R = 0.067$ ($\|F\| > 4\sigma$)
	$R_w = 0.363$ ($\|F\| > 4\sigma$)	$R_w = 0.312$ ($\|F\| > 4\sigma$)	$R_I = 0.124$ (100 K)	$R_w = 0.200$ ($\|F\| > 4\sigma$)

at beamline BL02B1 of the SPring-8 large SR facility [25]. The crystal structures were determined by using *SIR* [26], *SHELX* [27] and *SP* [28]. The experimental conditions and crystallographic data are summarized in table 1 and crystallographic information files (CIFs) as the electronic supplementary material. The CIF deposition numbers at the Cambridge Crystallographic Data Centre (CCDC) are 1826722 for [Li^+@C_{60}]($TFPB^-$), 1826723 for [Li^+@C_{60}]($TFSI^-$) and 1826724 for [Li^+@$C_{60}{}^-$](NiOEP).

3. Results and discussion

3.1. [Li^+@C_{60}]($TFPB^-$)·$C_4H_{10}O$

Figure 1 shows the crystal structure of [Li^+@C_{60}]($TFPB^-$) containing diethyl ether ($C_4H_{10}O$) solvent molecules at 260 K. The crystal shows a structural phase transition with a non-merohedral twinning around 250 K. The crystal structure above the phase transition temperature was determined in this study. The monoclinic lattice constants ($a = 17.11$ Å, $b = 20.38$ Å, $c = 19.89$ Å, $\beta = 105.16°$) and molecular arrangement are rather different from those of a solvent-free crystal ($a = 13.40$ Å, $b = 26.03$ Å, $c = 17.03$ Å, $\beta = 90.52°$) reported in [21]. The volume of the unit cell containing four [Li^+@C_{60}]($TFPB^-$) ion pairs for the solvent-containing crystal (6697 Å^3) is larger than that for the solvent-free crystal (5939 Å^3). As a result, the coordination structures around the Li^+@C_{60} are different between the solvent-free and solvent-containing crystals. The C_{60} centres are in the general positions of monoclinic structures in both crystals. The Li^+@C_{60} molecule in the solvent-free crystal is coordinated by six $TFPB^-$ anions with an octahedral arrangement. The distance from the C_{60} centre to the nearest central boron atom of $TFPB^-$ is 8.1 Å. The distance from the C_{60} centre to the nearest C_{60} centre is 11.4 Å. The crystal structure of the solvent-containing [Li^+@C_{60}]($TFPB^-$) consists of one-dimensional Li^+@C_{60} arrays and $TFPB^-$ arrays along the

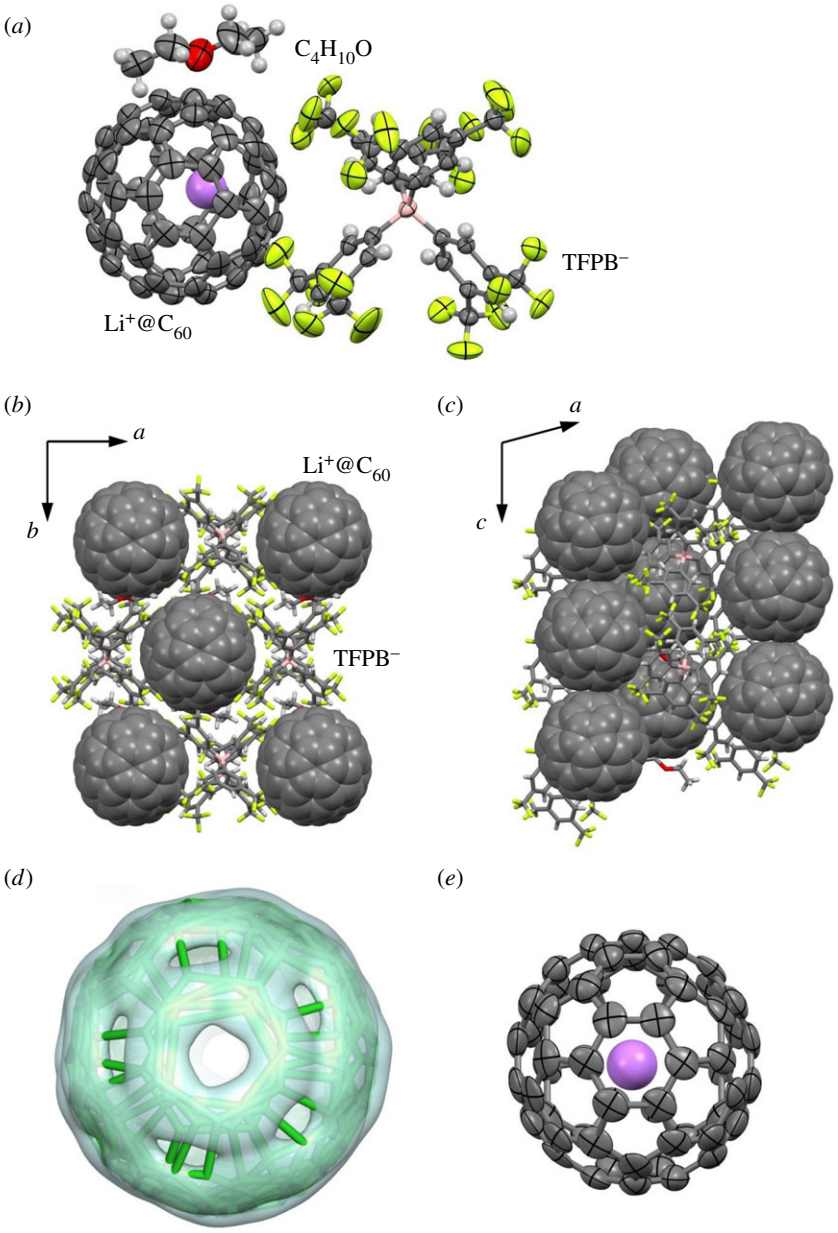

Figure 1. Crystal structure of $[Li^{+}@C_{60}](TFPB^{-})\cdot C_4H_{10}O$ at 260 K. (*a*) Structure with thermal ellipsoids at the 50% probability level viewed along the *c*-axis. Hydrogen atoms are drawn as small spheres. Disordered structures are omitted. (*b*) Molecular arrangement viewed along the *c*-axis. (*c*) Molecular arrangement viewed along the *b*-axis. (*d*) Disordered structure of the C_{60} cage with the electron charge-density surface at 1.5 $e/Å^3$ obtained by the maximum entropy method. A pentagon of the major orientation and four hexagons of the minor orientations are overlapping in the structure. (*e*) Structure of $Li^{+}@C_{60}$ with thermal ellipsoids at the 50% probability level viewed perpendicular to a hexagon near the violet encapsulated Li^{+} cation.

c-axis, as shown in figure 1*b*,*c*. The distance from the C_{60} centres to the nearest central boron atom of $TFPB^{-}$ is 8.7 Å. The distance from the C_{60} centre to the nearest two C_{60} centres along the *c*-axis is 10.0 Å. Therefore, $Li^{+}@C_{60}$ to $TFPB^{-}$ distances are increased and $Li^{+}@C_{60}$ to $Li^{+}@C_{60}$ distances are decreased by intercalation of $C_4H_{10}O$ solvent molecules.

The differences in coordination structure around $Li^{+}@C_{60}$ between the solvent-free and solvent-containing crystals affect the rotational motion of the C_{60} cages. Fullerene molecules often show rotational motion and orientation disorder in crystals. For instance, C_{60} cages in $[Li^{+}@C_{60}](PF_6^{-})$ and pristine C_{60} crystals show free rotational motion at high temperature [18,29]. The free rotational motions are stopped at low temperature by phase transitions at 370 K in $[Li^{+}@C_{60}](PF_6^{-})$ and 260 K in pristine C_{60}. Although the C_{60} orientation is perfectly ordered in the low temperature $[Li^{+}@C_{60}](PF_6^{-})$ [18],

orientation disorder with two molecular orientations remains in the low-temperature pristine C_{60} [30,31]. This suggests that rotational motion of the C_{60} cages is hindered by electrostatic interactions between the cationic $Li^+@C_{60}$ and coordinated anions. C_{60} cages in the reported crystal structure of the solvent-free $[Li^+@C_{60}](TFPB^-)$ show no orientation disorder [21]. The electrostatic interactions between $Li^+@C_{60}$ and $TFPB^-$ should be weakened by the increase in $Li^+@C_{60}$ to $TFPB^-$ distances by intercalation of $C_4H_{10}O$ solvent molecules. As a result, C_{60} cages in the solvent-containing $[Li^+@C_{60}](TFPB^-)$ crystal show a severe orientation disorder with five molecular orientations, as shown in figure 1*d*. The site occupancies for the five C_{60} orientations are 0.372(5), 0.253(4), 0.155(4), 0.132(3) and 0.124(4).

A weak electron charge-density peak for an Li^+ cation was observed inside the disordered C_{60} cage of the solvent-containing $[Li^+@C_{60}](TFPB^-)$ at 260 K. The Li^+ position at $(x, y, z) = (0.235, 0.758, 0.151)$ is close to the gravity centre at (0.228, 0.741, 0.147) for the central boron atoms of the six $TFPB^-$ anions adjacent to the $Li^+@C_{60}$ with an interval of 0.13 Å, and, hence, the Li^+ position is electrostatically consistent with the anion arrangement. The Li^+ position is beneath the centre of a hexagon of the C_{60} with the major orientation, as shown in figure 1*e*. The average Li^+–C distance is 2.35(10) Å, which agrees with the value for $[Li^+@C_{60}](PF_6^-)$ at low temperature [18,19]. Assuming that the site occupancy for the Li^+ position is the same as that of the major C_{60} orientation (0.372(5)), the isotropic atomic displacement parameter of the Li^+ is refined to 0.24(3) $Å^2$, and the remaining fraction of the Li^+ cation would occupy other positions inside the C_{60} by a positional disorder. The Li^+ position in the solvent-free $[Li^+@C_{60}](TFPB^-)$ has not been determined even at 123 K [21]. The Li^+ cation of cubic $[Li@C_{60}](PF_6^-)$ is freely rotating on a shell with a radius of 1.5 Å inside the C_{60} cage above 100 K [18–20]. Therefore, the Li^+ cation is partially ordered in the solvent-containing $[Li^+@C_{60}](TFPB^-)$ by the asymmetric coordination of $TFPB^-$ anions and $C_4H_{10}O$ molecules, as shown in figure 1*b*,*c*.

3.2. $[Li^+@C_{60}](TFSI^-)\cdot CH_2Cl_2$

Figure 2 shows the crystal structure of $[Li^+@C_{60}](TFSI^-)$ containing dichloromethane (CH_2Cl_2) solvent molecules at 150 K. The crystal shows a structural phase transition with a non-merohedral twinning around 130 K. The crystal structure above the phase transition temperature was determined in this study. The $TFSI^-$ anion and CH_2Cl_2 molecule are polar molecules, while the $TFPB^-$, ClO_4^-, $SbCl_6^-$ and PF_6^- anions are non-polar molecules. Permanent electric dipole moments of such polar molecules should electrostatically interact with the Li^+ cations inside the C_{60} cages in crystals. However, the electric dipole moments of $TFSI^-$ and CH_2Cl_2 are cancelled by the antiferroelectric arrangements in the crystal structure with a non-polar space group of *Pnma*. If an $Li^+@C_{60}$ crystal containing polar anions with a polar space group was obtained, the crystal could have a macroscopic electric dipole moment and exhibit ferroelectricity due to a switching of the polar anions and motion of the Li^+ cations. Ferroelectric crystals of C_{60} encapsulating a polar molecule have been predicted theoretically [32]. Actually, a cubic crystal of C_{60} with a polar water molecule inside ($H_2O@C_{60}$) shows an increase in the dielectric permittivity according to the Curie–Weiss law at low temperature, although no ferroelectric phase transition is observed down to 8 K [33].

The molecular arrangement of $Li^+@C_{60}$ molecules in the *bc*-plane shown in figure 2*b* is similar to that of $[Li^+@C_{60}](TFPB^-)\cdot C_4H_{10}O$ in the *ab*-plane shown in figure 1*b* and the face-centred molecular arrangement in $[Li^+@C_{60}](PF_6^-)$. The lattice constants for $b = 13.89$ Å and $c = 13.96$ Å for $[Li^+@C_{60}](TFSI^-)\cdot CH_2Cl_2$ at 150 K are much smaller than $a = 17.11$ Å and $b = 20.38$ Å for $[Li^+@C_{60}](TFPB^-)\cdot C_4H_{10}O$ at 260 K, and comparable to the cubic lattice constant of $a = 14.30$ Å for $[Li^+@C_{60}](PF_6^-)$ at 150 K. The monolayer lattice in the *bc*-plane of $[Li^+@C_{60}](TFSI^-)\cdot CH_2Cl_2$ is stacked along the *a*-axis with a shift to the *c*-axis. If the shift is 0, the $Li^+@C_{60}$ arrangement becomes similar to that in $[Li^+@C_{60}](TFPB^-)\cdot C_4H_{10}O$, as shown in figure 1*b*,*c*. If the shift is $c/2$, the $Li^+@C_{60}$ arrangement becomes similar to the face-centred molecular arrangement in $[Li^+@C_{60}](PF_6^-)$. Therefore, the molecular arrangements of $[Li^+@C_{60}](TFPB^-)\cdot C_4H_{10}O$ (figure 1*b*,*c*) and $[Li^+@C_{60}](TFSI^-)\cdot CH_2Cl_2$ (figure 2*b*,*c*) can be classified into deformed rock-salt-type structures.

C_{60} cages in $[Li^+@C_{60}](TFSI^-)\cdot CH_2Cl_2$ also show a severe orientation disorder, as shown in figure 2*d*. The C_{60} cage was modelled by an overlap of three partially occupied C_{60} cages with different orientations. The site occupancies for the three C_{60} orientations are 0.413(3), 0.413(3) and 0.174(5). The two major orientations are equivalent to the crystallographic mirror symmetry. The number of overlapping orientations is less than that in $[Li^+@C_{60}](TFPB^-)\cdot C_4H_{10}O$ (figure 1*d*). The orientation disorder of C_{60} is strongly affected by the exchange of anion and solvent molecules and is suppressed at low temperature. Anion exchange from larger $TFPB^-$ to smaller $TFSI^-$ should increase the van der Waals inter-fullerene interactions and electrostatic Li^+–anion interactions. The measurement temperature of

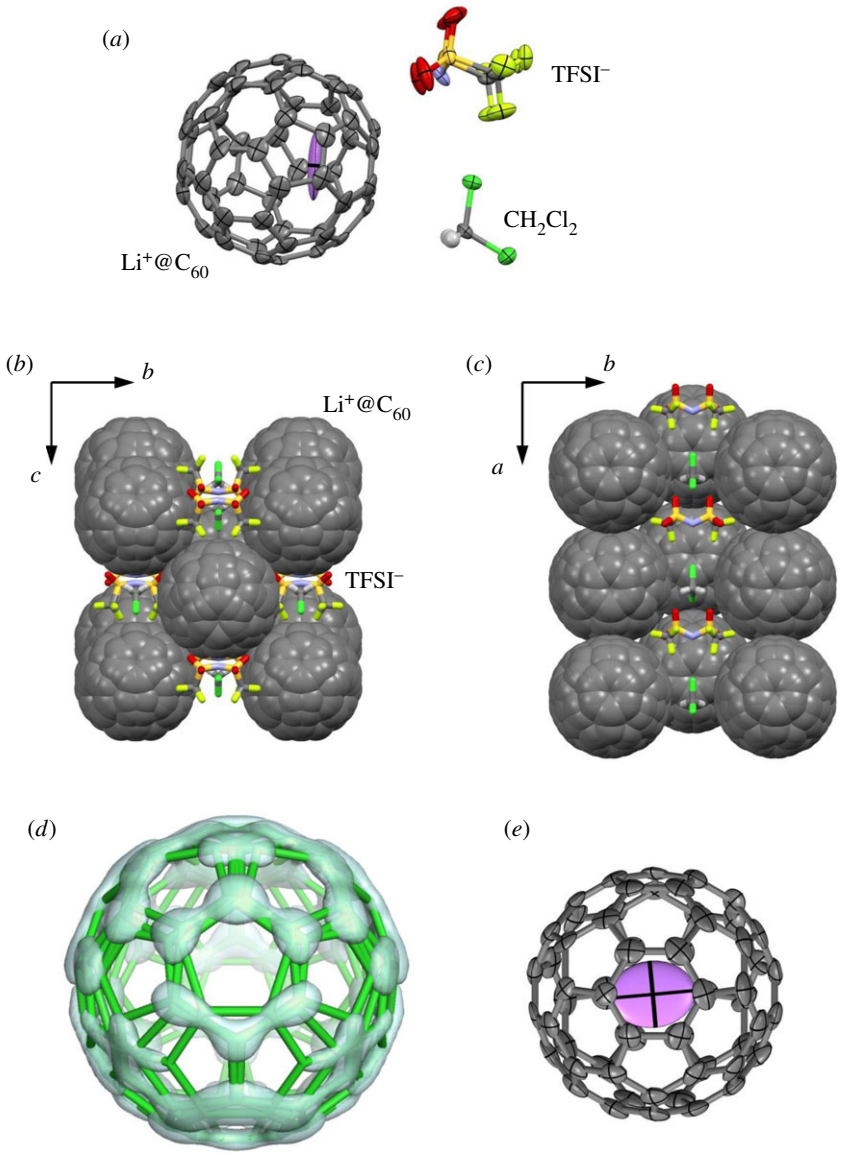

Figure 2. Crystal structure of $[Li^+@C_{60}](TFSI^-)\cdot CH_2Cl_2$ at the 150 K. (*a*) Structure with thermal ellipsoids at the 50% probability level viewed along the *b*-axis. Hydrogen atoms are drawn as small spheres. Disordered structures are omitted. (*b*) Molecular arrangement viewed along the *a*-axis. (*c*) Molecular arrangement viewed along the *c*-axis. (*d*) Disordered structure of the C_{60} cage with the electron charge-density surface at 1.7 $e/Å^3$ obtained by the maximum entropy method. Two hexagons of the major orientations and a pentagon of the minor orientation are overlapping in the structure. (*e*) Structure of $Li^+@C_{60}$ with thermal ellipsoids at the 50% probability level viewed perpendicular to a hexagon near the violet encapsulated Li^+ cation.

$[Li^+@C_{60}](TFSI^-)\cdot CH_2Cl_2$ (150 K) is also lower than that of $[Li^+@C_{60}](TFPB^-)\cdot C_4H_{10}O$ (260 K). These are reasons for the suppression of C_{60} orientation disorder in $[Li^+@C_{60}](TFSI^-)\cdot CH_2Cl_2$. On the other hand, C_{60} cages in the solvent-free $[Li^+@C_{60}](TFPB^-)$ show no orientation disorder [21]. It is expected that C_{60} orientations are also ordered in solvent-free $[Li^+@C_{60}](TFSI^-)$.

The Li^+ cation in $[Li^+@C_{60}](TFSI^-)\cdot CH_2Cl_2$ also locates beneath the centre of a hexagon of the C_{60} with the major orientation, as shown in figure 1*e*. The average Li^+–C distance of 2.42(7) Å is consistent with that in $[Li^+@C_{60}](TFPB^-)\cdot C_4H_{10}O$. The Li^+ position at (0.803, 0.750, 0.040) is close to the gravity centre at (0.763, 0.750, 0.083) for central nitrogen atoms of the six $TFSI^-$ anions adjacent to the $Li^+@C_{60}$ with an interval of 0.98 Å, and, hence, the Li^+ position is electrostatically consistent with the anion arrangement. The flat thermal ellipsoid for the Li^+ cation with a site occupancy of 1.0 suggests a large librational motion of the Li^+ cation. The free rotational motion and positional disorder of the Li^+ cation in $[Li^+@C_{60}](PF_6^-)$ and solvent-free and solvent-containing $[Li^+@C_{60}](TFPB^-)$ will be suppressed by anion exchange from non-polar PF_6^- and $TFPB^-$ anions to polar $TFSI^-$ anions.

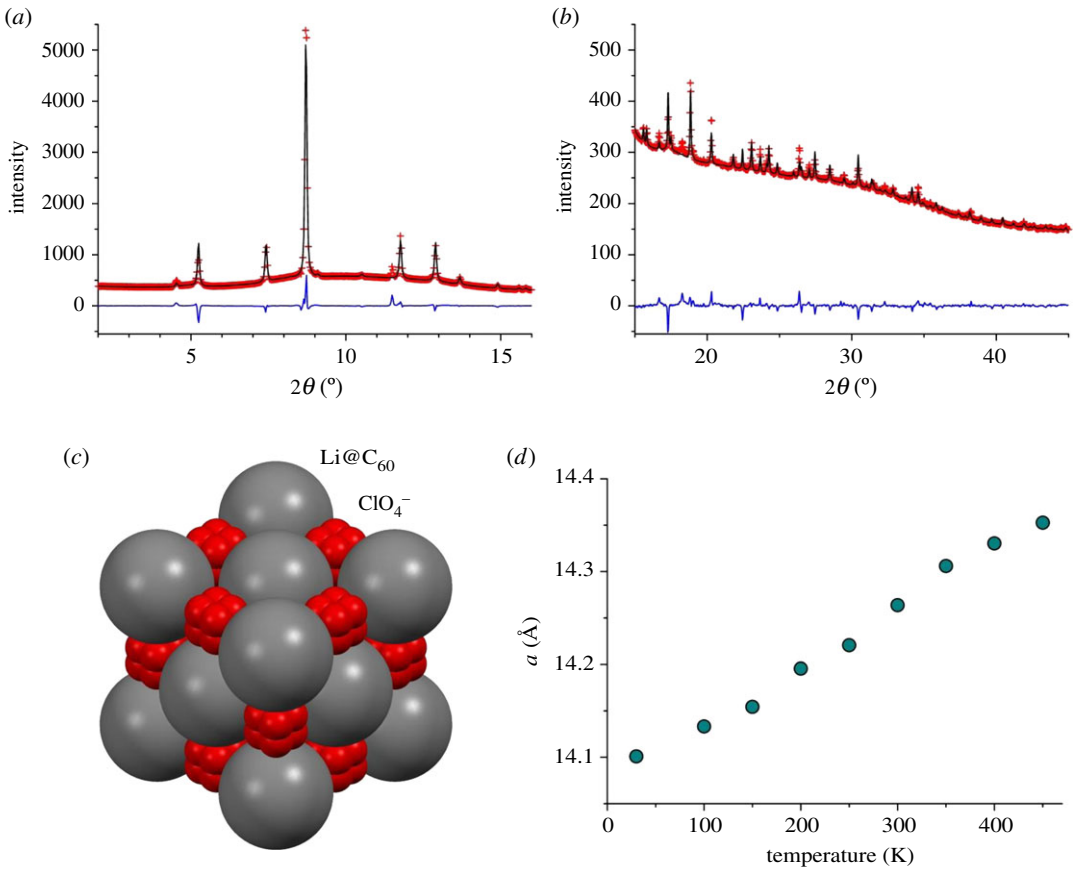

Figure 3. (*a*,*b*) Powder XRD pattern of $[Li^{+}@C_{60}](ClO_4^{-})$ at 100 K (X-ray wavelength: 0.649 Å) with a fitting result by the Rietveld refinement. Observed and calculated intensities are plotted by red crosses and black lines, respectively. Deviations between observed and calculated intensities are plotted by blue lines. Low and high 2θ angle regions are shown separately in (*a*) and (*b*), respectively. (*c*) Crystal structure model of $[Li^{+}@C_{60}](ClO_4^{-})$ viewed along the threefold inversion axis. Grey and red spheres are uniform C_{60} shells and oxygen atoms of disordered ClO_4^{-} anions, respectively. (*d*) Temperature dependence of the cubic lattice constant of $[Li^{+}@C_{60}](ClO_4^{-})$ from 30 to 450 K.

3.3. $[Li^{+}@C_{60}](ClO_4^{-})$

Figure 3*a*,*b* shows the powder XRD pattern of $[Li^{+}@C_{60}](ClO_4^{-})$ at 100 K (X-ray wavelength: 0.649 Å) with a fitting result by the Rietveld refinement. A face-centred-cubic (fcc) structure model similar to the crystal structure of $[Li^{+}@C_{60}](PF_6^{-})$ above 370 K was used in the refinement. $[Li^{+}@C_{60}](PF_6^{-})$ and pristine C_{60} undergo a phase transition from the fcc structure (space group: $Fm\bar{3}m$) to the low-temperature simple-cubic structure (space group: $Pa\bar{3}$) at 370 K and 260 K, respectively [18,29]. Surprisingly, $[Li^{+}@C_{60}](ClO_4^{-})$ has an fcc structure even at 100 K. The cubic lattice constant of $[Li^{+}@C_{60}](ClO_4^{-})$ is $a = 14.13$ Å at 100 K, which is smaller than that of $[Li^{+}@C_{60}](PF_6^{-})$ at 100 K ($a = 14.28$ Å) and larger than that of pristine C_{60} at 100 K ($a = 14.06$ Å) [18,31]. This relationship is consistent with the fact that a ClO_4^{-} anion is smaller than a PF_6^{-} anion.

Figure 3*c* shows the crystal structure model used in the powder pattern fitting. The space group is $Fm\bar{3}m$. The uniform spherical C_{60} shell with a radius of 3.55 Å centred at 0, 0, 0 and the disordered ClO_4^{-} anion centred at 1/2, 1/2, 1/2 form a rock-salt-type cubic structure. The disordered ClO_4^{-} anion was modelled by a Cl atom at 1/2, 1/2, 1/2 and partially occupied O atoms at $1/2 \pm 0.059$, $1/2 \pm 0.059$, $1/2 \pm 0.059$ with a site occupancy of 1/2. The disordered structure is given by orthogonal overlap of two ClO_4^{-} tetrahedra with a Cl–O distance of 1.44 Å. The powder pattern was fitted by using the simple structure model with acceptable reliable factors ($R_{wp} = 0.036$, $R_I = 0.124$). However, the reliable Li^{+} position could not be determined due to the multi-site occupation or free rotational motion. The remaining deviations between the observed and calculated intensities in figure 3*a*,*b* are mainly due to non-uniformity of the electron charge densities on the C_{60} shell.

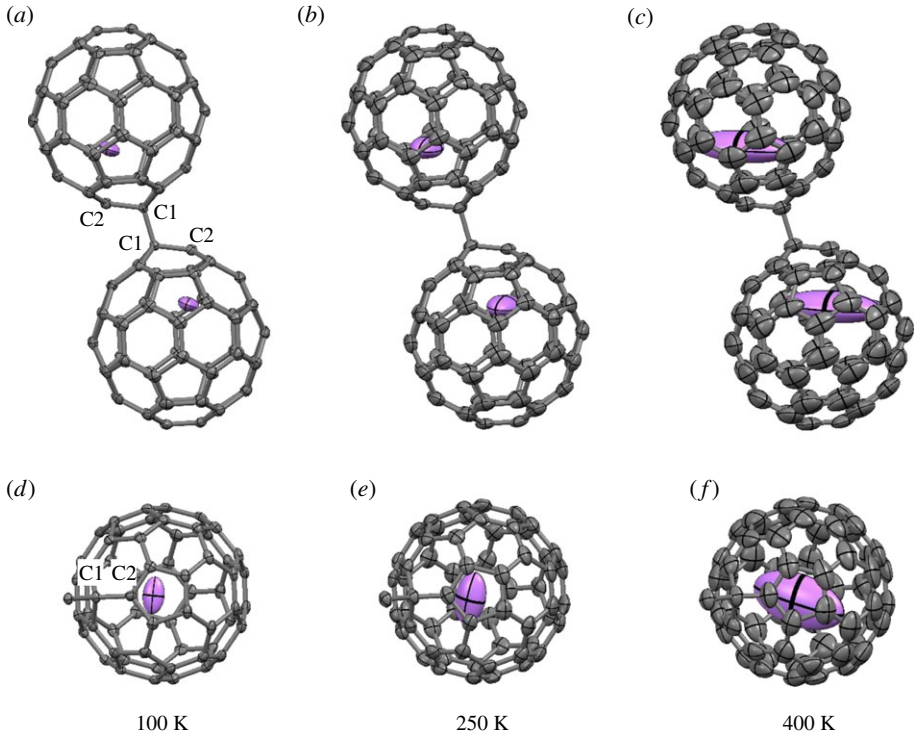

Figure 4. Molecular structure of the $(Li^{+}@C_{60}^{-})_2$ dimer in $[Li^{+}@C_{60}^{-}](NiOEP)\cdot CH_2Cl_2$ at (*a*,*d*) 100, (*b*,*e*) 250 and (*c*,*f*) 400 K. (*a*–*c*) View perpendicular to the inter-fullerene single C1–C1 bond. (*d*–*f*) View perpendicular to a pentagon near the violet encapsulated Li^{+} cation. The thermal ellipsoids are drawn at the 50% probability level. Disordered structures at 250 and 400 K and coordinated NiOEP and CH_2Cl_2 molecules are omitted.

Figure 3*d* shows the temperature dependence of the cubic lattice constant of $[Li^{+}@C_{60}](ClO_4^{-})$ from 30 to 450 K. No phase transition was observed in the temperature range. A ternary alkali-doped fulleride Li_2CsC_{60} also shows no phase transition and has an fcc structure from 50 to 300 K [34]. Disordered occupation of small Li^{+} and large Cs^{+} cations at tetrahedral voids at 1/4, 1/4, 1/4 and octahedral voids at 1/2, 1/2, 1/2 would hinder the orientation ordering of C_{60} at low temperature in Li_2CsC_{60}. By contrast, tetrahedral ClO_4^{-} anions occupy the octahedral voids in $[Li^{+}@C_{60}](ClO_4^{-})$, as shown in figure 3*c*. The mismatch between the molecular symmetry and the site symmetry would hinder the orientation ordering of ClO_4^{-} and C_{60} at low temperature in $[Li@C_{60}](ClO_4^{-})$. $[Li^{+}@C_{60}](PF_6^{-})$, in which octahedral PF_6^{-} anions occupy the octahedral voids, shows perfect orientation ordering of C_{60} below 370 K [18].

3.4. $[Li^{+}@C_{60}^{-}](NiOEP)\cdot CH_2Cl_2$

Figure 4 shows the temperature dependence of the molecular structure of the single-bonded $(Li^{+}@C_{60}^{-})_2$ dimer in $[Li^{+}@C_{60}^{-}](NiOEP)\cdot CH_2Cl_2$. The $(Li^{+}@C_{60}^{-})_2$ dimer has a disordered structure by a ratchet-type rotation along the inter-fullerene single C–C bond with a rotation angle of about 39° above the phase transition temperature around 250 K [22]. The disordered structures at 250 and 400 K are omitted in the figure. $(C_{60}^{-})_2$ dimers in complex crystals of C_{60} with donor and solvent molecules dissociate above 160–220 K [35,36]. By contrast, the $(Li^{+}@C_{60}^{-})_2$ dimers in $[Li^{+}@C_{60}^{-}](NiOEP)\cdot CH_2Cl_2$ are thermally stable even at 400 K, as shown in figure 4*c*. It is suggested that the inter-fullerene single C–C bond is stabilized by the encapsulation of Li^{+} cations. Low stability of $(C_{60}^{-})_2$ dimers is due to the strong repulsion of two negative charges within the dimer. The Li^{+} cation inside the cage which compensates this negative charge contributes essential stabilization of $(Li^{+}@C_{60}^{-})_2$ dimers.

The encapsulated Li^{+} cation is localized with a site occupancy of 1.0 near the carbon atom (C2) nearest to the carbon atom (C1) forming the inter-fullerene single C–C bond (figure 4*a*). The Li^{+}–C2 distance is 2.21(1), 2.31(2) and 2.36(6) Å at 100, 250 and 400 K, respectively. The value at 100 K is obviously shorter than the Li^{+}–C distance of 2.37(1) Å in $[Li^{+}@C_{60}](PF_6^{-})$ at 40 K [19]. It is also noted that the Li^{+} cation in the $(Li^{+}@C_{60}^{-})_2$ dimer locates near the centre of a pentagon involving C2, as shown in figure 4*d*,*e*,

while the Li^+ cation in $[Li^+@C_{60}](PF_6^-)$ locates near the centre of the hexagons [18,19]. The formation of the shorter Li^+–C bond contributes to stabilization of the $(Li^+@C_{60}^-)_2$ dimer. The inter-fullerene C1–C1 distance shows almost no temperature dependence, which are 1.59(1), 1.59(1) and 1.60(1) Å at 100, 250 and 400 K, respectively.

The thermal ellipsoid of the Li^+ cation is unusually large perpendicular to the radial direction from the C_{60} centre at 400 K (figure 4*c,f*). The equivalent atomic displacement parameters of the Li^+ cation and C2 atom are 0.8(1) and 0.077(2) $Å^2$, respectively. The thermally induced large librational motion of the Li^+ cation in the $(Li^+@C_{60}^-)_2$ dimer is basically consistent with the free rotational motion of the Li^+ cation in $[Li^+@C_{60}](PF_6^-)$ above 100 K. The Li^+ cation bonded to the C2 atom cannot rotate freely in the $(Li^+@C_{60}^-)_2$ dimer even at 400 K.

4. Conclusion

We determined structures of cationic $Li^+@C_{60}$ monomers and neutral $(Li^+@C_{60}^-)_2$ dimers in crystals by SR XRD measurements to understand the electrostatic and thermal properties of the encapsulated Li^+ cation. $[Li^+@C_{60}](TFPB^-)\cdot C_4H_{10}O$ and $[Li^+@C_{60}](TFSI^-)\cdot CH_2Cl_2$ involve severe orientation disorder of the C_{60} cages at low temperature. However, the Li^+ cations are rather ordered at specific positions by electrostatic interactions from non-polar $TFPB^-$ or polar $TFSI^-$ anions, which asymmetrically coordinate to the C_{60} cage. $[Li^+@C_{60}](ClO_4^-)$ has a rock-salt-type cubic structure similar to the structure of $[Li^+@C_{60}](PF_6^-)$. The $Li^+@C_{60}$ molecules in $[Li^+@C_{60}](ClO_4^-)$ are fully disordered with almost uniform spherical shell charge densities by octahedral coordination of ClO_4^- tetrahedra even at 100 K, and show no orientation ordering or structural phase transition unlike $[Li^+@C_{60}](PF_6^-)$ and pristine C_{60}. Single-bonded $(Li^+@C_{60}^-)_2$ dimers in $[Li^+@C_{60}^-](NiOEP)\cdot CH_2Cl_2$ are stable even at 400 K, while $(C_{60}^-)_2$ dimers in a complex of C_{60} dissociate. The formation of Li^+–C bonds, which are shorter and thermally more stable than Li^+–C bonds in $[Li^+@C_{60}](PF_6^-)$, stabilizes the inter-fullerene single C–C bond and suppresses the free rotational motion of the Li^+ cation. The variety of structures of $Li^+@C_{60}$ revealed in this study proves the controllability of the position and motion of the encapsulated Li^+ cation from outside the C_{60} cage, which would be valuable in future applications of $Li^+@C_{60}$ as molecular devices. This study shows that the spherical $Li^+@C_{60}$ cation forms various ionic crystals with common inorganic and organic anions, and the neutral $Li^+@C_{60}^-$ consisting of a positive Li^+ core and a negative C_{60}^- cage forms thermally stable molecular crystals of covalently bonded $(Li^+@C_{60}^-)_2$ dimers. The results are essential and important to support the strong superatomic character of $Li^+@C_{60}$.

Data accessibility. The CIFs are available as the electronic supplementary material and from the Cambridge Crystallographic Data Centre (CCDC) (www.ccdc.cam.ac.uk/structures) with deposition numbers 1826722, 1826723 and 1826724.

Authors' contributions. S.A. carried out the SR XRD experiments and crystal structure analyses, and wrote the manuscript. K.M. carried out the crystallization and crystal structure analysis. H.U. and H.O. carried out the anion exchange, electrochemical reduction and crystallization. Y.M. and K.K. supervised and conducted the sample preparations and chemical analyses. All authors gave final approval for publication.

Competing interests. We declare we have no competing interests.

Funding. This work was financially supported by The Mitsubishi Foundation and The Murata Science Foundation.

Acknowledgements. The synchrotron radiation experiments were performed at SPring-8 with the approval of the Japan Synchrotron Radiation Research Institute (JASRI) (proposal nos. 2013A0100, 2013B0100, 2015A0100, 2017A1206 and 2017A1739). S.A. thanks Mr Y. Yokoi, Ms Y. Nakahira and Dr K. Sugimoto for their help with the experiments.

References

1. Shinohara H. 2000 Endohedral metallofullerenes. *Rep. Prog. Phys.* **63**, 843–892. (doi:10.1088/0034-4885/63/6/201)
2. Popov AA, Yang S, Dunsch L. 2013. Endohedral fullerenes. *Chem. Rev.* **113**, 5989–6113. (doi:10.1021/cr300297r)
3. Harneit W. 2002 Fullerene-based electron-spin quantum computer. *Phys. Rev. A* **65**, 032322. (doi:10.1103/PhysRevA.65.032322)
4. Morton JJL, Tyryshkin AM, Ardavan A, Benjamin SC, Porfyrakis K, Lyon SA, Briggs GAD. 2006 Bang–bang control of fullerene qubits using ultrafast phase gates. *Nat. Phys.* **2**, 40–43. (doi:10.1038/nphys192)
5. Mikawa M, Kato H, Okumura M, Narazaki M, Kanazawa Y, Miwa N, Shinohara H. 2001 Paramagnetic water-soluble metallofullerenes having the highest relaxivity for MRI contrast agents. *Bioconjug. Chem.* **12**, 510–514. (doi:10.1021/bc000136m)
6. Bolskar RD, Benedetto AF, Husebo LO, Price RE, Jackson EF, Wallace S, Wilson LJ, Alford JM. 2003 First soluble $M@C_{60}$ derivatives provide enhanced access to metallofullerenes and permit in vivo evaluation of $Gd@C_{60}[C(COOH)_2]_{10}$ as a MRI contrast agent. *J. Am. Chem. Soc.* **125**, 5471–5478. (doi:10.1021/ja0340984)
7. Yasutake Y, Shi Z, Okazaki T, Shinohara H, Majima Y. 2005 Single molecular orientation switching of an endohedral metallofullerene. *Nano Lett.* **5**, 1057–1060. (doi:10.1021/nl050490z)
8. Huang T, Zhao J, Feng M, Popov AA, Yang S, Dunsch L, Petek H. 2011 A molecular switch based on current-driven rotation of an encapsulated cluster within a fullerene cage. *Nano Lett.* **11**, 5327–5332. (doi:10.1021/nl2028409)

9. Thompson BC, Fréchet JM. 2008 Polymer-fullerene composite solar cells. *Angew. Chem. Int. Ed.* **47**, 58–77. (doi:10.1002/anie.200702506)
10. Nelson J. 2011 Polymer:fullerene bulk heterojunction solar cells. *Mater. Today* **14**, 462–470. (doi:10.1016/S1369-7021(11)70210-3)
11. Aoyagi S *et al.* 2010 A layered ionic crystal of polar Li@C_{60} superatoms. *Nat. Chem.* **2**, 678–683. (doi:10.1038/nchem.698)
12. Okada H *et al.* 2012 Preparation of endohedral fullerene containing lithium (Li@C_{60}) and isolation as pure hexafluorophosphate salt ([Li^+@C_{60}][PF_6^-]). *RSC Adv.* **2**, 10 624–10 631. (doi:10.1039/C2RA21244G)
13. Matsuo Y, Okada H, Ueno H. 2017 *Endohedral lithium-containing fullerenes: preparation, derivatization, and application*. Singapore: Springer.
14. Fukuzumi S, Ohkubo K. 2013 Long-lived photoinduced charge separation for solar cell applications in supramolecular complexes of multi-metalloporphyrins and fullerenes. *Dalton. Trans.* **42**, 15 846–15 858. (doi:10.1039/C3DT51883C)
15. Ohkubo K, Kawashima Y, Sakai H, Hasobe T, Fukuzumi S. 2014 Enhanced photoelectrochemical performance of composite photovoltaic cells of Li^+@C_{60}^- sulphonated porphyrin supramolecular nanoclusters. *Chem. Commun.* **49**, 4474–4476. (doi:10.1039/C3CC41187G)
16. Sakai H, Kamimura T, Tani F, Hasobe T. 2015 Supramolecular photovoltaic cells utilizing inclusion complexes composed of Li^+@C_{60} and cyclic porphyrin dimer. *J. Porphyr. Phthalocyanines* **19**, 242–250. (doi:10.1142/S1088424614501156)
17. Tran CM, Sakai H, Kawashima Y, Ohkubo K, Fukuzumi S, Murata H. 2017 Multi-level non-volatile organic transistor-based memory using lithium-ion-encapsulated fullerene as a charge trapping layer. *Org. Electron.* **45**, 234–239. (doi:10.1016/j.orgel.2017.03.018)
18. Aoyagi S, Sado Y, Nishibori E, Sawa H, Okada H, Tobita H, Kasama Y, Kitaura R, Shinohara H. 2012 Rock-salt-type crystal of thermally contracted C_{60} with encapsulated lithium cation. *Angew. Chem. Int. Ed.* **51**, 3377–3381. (doi:10.1002/anie.201108551)
19. Aoyagi S, Tokumitu A, Sugimoto K, Okada H, Hoshino N, Akutagawa T. 2016 Tunneling motion and antiferroelectric ordering of lithium cations trapped inside carbon cages. *J. Phys. Soc. Jpn.* **85**, 094605. (doi:10.7566/JPSJ.85.094605)
20. Suzuki H, Ishida M, Yamashita M, Otani C, Kawachi K, Kasama Y, Kwon E. 2016 Rotational dynamics of Li^+ ions encapsulated in C_{60} cages at low temperatures. *Phys. Chem. Chem. Phys.* **18**, 31 384–31 387. (doi:10.1039/C6CP06949E)
21. Okada H, Matsuo Y. 2014 Anion exchange of Li^+@C_{60} salt for improved solubility. *Fullerenes Nanotubes Carbon Nanostruct.* **22**, 262–268. (doi:10.1080/1536383X.2013.812639)
22. Ueno H *et al.* 2016 Electrochemical reduction of cationic Li^+@C_{60} to neutral Li^+@C_{60}^-: isolation and characterisation of endohedral [60]fulleride. *Chem. Sci.* **7**, 5770–5774. (doi:10.1039/C6SC01209D)
23. Konarev DV, Zorina LV, Khasanov SS, Popov AA, Otsuka A, Yamochi H, Saito G, Lyubovskayaa RN. 2016 A crystalline anionic complex of scandium nitride endometallofullerene: experimental observation of single-bonded (Sc_3N@I_h — C_{80}^-)$_2$ dimers. *Chem. Commun.* **52**, 10 763–10 766. (doi:10.1039/c6cc05550h)
24. Voevodin A, Abella L, Castro E, Paley DW, Campos LM, Rodríguez-Fortea A, Poblet JM, Echegoyen L, Roy X. 2017 Dimerization of endohedral fullerene in a superatomic crystal. *Chem. Eur. J.* **23**, 13 305–13 308. (doi:10.1002/chem.201703203)
25. Sugimoto K, Ohsumi H, Aoyagi S, Nishibori E, Moriyoshi C, Kuroiwa Y, Sawa H, Takata M. 2010 Extremely high resolution single crystal diffractometory for orbital resolution using high energy synchrotron radiation at SPring-8. *AIP Conf. Proc.* **1234**, 887–890. (doi:10.1063/1.3463359)
26. Burla MC, Caliandro R, Carrozzini B, Cascarano GL, Cuocci C, Giacovazzo C, Mallamo M, Mazzone A, Polidori G. 2015 Crystal structure determination and refinement via SIR2014. *J. Appl. Cryst.* **48**, 306–309. (doi:10.1107/S1600576715001132)
27. Sheldrick GM. 2015 Crystal structure refinement with SHELXL. *Acta Cryst. C* **71**, 3–8. (doi:10.1107/S2053229614024218)
28. Nishibori E, Sunaoshi E, Yoshida A, Aoyagi S, Kato K, Takata M, Sakata M. 2007 Accurate structure factors and experimental charge densities from synchrotron X-ray powder diffraction data at SPring-8. *Acta. Cryst. A* **63**, 43–52. (doi:10.1107/S0108767306047210)
29. Heiney PA, Fischer JE, McGhie AR, Romanow WJ, Denenstein AM, McCauley Jr JP, Smith AB, Cox DE. 1991 Orientational ordering transition in solid C_{60}. *Phys. Rev. Lett.* **66**, 2911–2914. (doi:10.1103/PhysRevLett.66.2911)
30. David WIF, Ibberson RM, Matthewman JC, Prassides K, Dennis TJS, Hare JP, Kroto HW, Taylor R, Walton DRM. 1991 Crystal structure and bonding of ordered C_{60}. *Nature* **353**, 147–149. (doi:10.1038/353147a0)
31. David WIF, Ibberson RM, Dennis TJS, Hare JP, Prassides K. 1992 Structural phase transitions in the fullerene C_{60}. *Euro. Phys. Lett.* **18**, 219–225. (doi:10.1209/0295-5075/18/3/006)
32. Cioslowski J, Nanayakkara A. 1992 Endohedral fullerites: a new class of ferroelectric materials. *Phys. Rev. Lett.* **69**, 2871–2873. (doi:10.1103/PhysRevLett.69.2871)
33. Aoyagi S, Hoshino N, Akutagawa T, Sado Y, Kitaura R, Shinohara H, Sugimoto K, Zhang R, Murata Y. 2014 A cubic dipole lattice of water molecules trapped inside carbon cages. *Chem. Commun.* **50**, 524–526. (doi:10.1039/C3CC46683C)
34. Hirosawa I, Prassides K, Mizuki J, Tanigaki K, Gevaert M, Lappas A, Cockcroft JK. 1994 Orientational disorder of C_{60} in Li_2CsC_{60}. *Science* **264**, 1294–1297. (doi:10.1126/science.264.5163.1294)
35. Konarev DV, Khasanov SS, Otsuka A, Saito G. 2002 The reversible formation of a single-bonded (C_{60}^-)$_2$ dimer in ionic charge transfer complex: Cp*2Cr · C_{60}($C_6H_4Cl_2$)$_2$. The molecular structure of (C_{60}^-)$_2$. *J. Am. Chem. Soc.* **124**, 8520–8521. (doi:10.1021/ja0202614)
36. Konarev DV, Khasanov SS, Saito G, Otsuka A, Yoshida Y, Lyubovskaya RN. 2003 Formation of single-bonded (C_{60}^-)$_2$ and (C_{70}^-)$_2$ dimers in crystalline ionic complexes of fullerenes. *J. Am. Chem. Soc.* **125**, 10 074–10 083. (doi:10.1021/ja035546a)